

Light quark mass dependence of the $X(3872)$ in XEFT

M. Jansen,^{1,2} H.-W. Hammer,^{1,3,4} and Yu Jia^{2,5}

¹*Helmholtz-Institut für Strahlen- und Kernphysik,
Universität Bonn, 53115 Bonn, Germany*

²*Institute of High Energy Physics, Chinese Academy of Sciences, Beijing 100049, China*

³*Institut für Kernphysik, Technische Universität Darmstadt, 64289 Darmstadt, Germany*

⁴*ExtreMe Matter Institute EMMI, GSI Helmholtzzentrum für
Schwerionenforschung GmbH, 64291 Darmstadt, Germany*

⁵*Theoretical Physics Center for Science Facilities, Institute of High Energy Physics,
Chinese Academy of Sciences, Beijing 100049, China*

(Dated: March 25, 2022)

Abstract

The quark mass dependence of hadrons is an important input for lattice calculations. We investigate the light quark mass dependence of the binding energy of the $X(3872)$ and the $\bar{D}^0 D^{*0}$ scattering length in the $C = +1$ channel to next-to-leading order in XEFT where pion interactions are perturbative. At this order, the quark mass dependence is determined by a quark mass-dependent contact interaction in addition to the one-pion exchange. Using naturalness arguments to constrain unknown parameters, we find a moderate sensitivity of the binding energy for quark masses up to twice the physical value while the scattering length is more sensitive. The occurrence of infrared divergences due to on-shell pions in XEFT and their treatment is discussed in detail.

PACS numbers: 14.40.Pq, 13.75.Lb, 11.30.Rd

I. INTRODUCTION

The discovery of a flurry of new quarkonium-like hadrons in the last decade has created exciting prospects in quarkonium physics [1]. In 2003, the Belle Collaboration discovered a charmonium-like hadron [2], known as the $X(3872)$, which was quickly confirmed by the CDF collaboration [3]. Its observed decays into $J/\psi\gamma$ imply even charge parity [4]. Ending a long discussion about its quantum numbers, the LHCb experiment was recently able to determine parity and total angular momentum, assigning the quantum numbers $J^{PC} = 1^{++}$ to the $X(3872)$ [5].

The quantum numbers and the proximity of the mass of the $X(3872)$ to the $\bar{D}^0 D^{*0}$ threshold suggest its interpretation as a loosely-bound S -wave hadronic molecule of $D^{(*)}$ mesons with the particle content [6–11]

$$X = \frac{1}{\sqrt{2}} (\bar{D}^0 D^{*0} + D^0 \bar{D}^{*0}). \quad (1)$$

The binding energy of the molecule, E_X , is then given as the difference of the sum of the masses of the D^0 and D^{*0} meson, m_D and m_{D^*} , and the mass of the $X(3872)$, M_X . Using the latest values from the review of particle properties [12], we obtain

$$E_X = m_{D^*} + m_D - M_X = (0.17 \pm 0.26) \text{ MeV}. \quad (2)$$

This energy E_X is small compared to the natural energy scale set by one-pion exchange, $m_\pi^2/(2M_{DD^*}) \approx 10$ MeV, where M_{DD^*} is the reduced mass of the D^0 and D^{*0} mesons. Thus the $X(3872)$ displays universal properties determined by its small binding energy or, equivalently, the large $\bar{D}^0 D^{*0}$ S -wave scattering length $a_s = \sqrt{2M_{DD^*} E_X}$ [13]. The exploration of this universality for the X using effective field theory methods was initiated by Braaten and Kusunoki [10]. A number of predictions for production amplitudes, decays, formation, and line shapes of the $X(3872)$ were obtained within this framework (see Ref. [14] for a review). The influence of three-body $D\bar{D}\pi$ interactions on the properties of the $X(3872)$ was found to be moderate in a Faddeev approach [15]. Finally, we note that universality also determines the interactions of the $X(3872)$ with neutral D and D^* mesons [16].

The corrections to universality can be calculated systematically using an effective field theory for the X with explicit pions, called XEFT, which was developed by Fleming, Kusunoki, Mehen and van Kolck in 2007 [17]. They applied XEFT to calculate the partial decay width $\Gamma[X \rightarrow D^0 \bar{D}^0 \pi^0]$ at next-to-leading order (NLO) in the XEFT power counting. Later, their work was extended to describe hadronic decays of the $X(3872)$ to the χ_{cJ} [18]. In Ref. [19], it was pointed out that XEFT can also be extended to systems with an additional pion with energies close to the $D^* \bar{D}^*$ threshold. As an example, the cross section for the breakup of the X into $D^{*+} \bar{D}^{*0}$ in the scattering of a low-energy charged pion was calculated.

In its structure, XEFT is similar to the Kaplan-Savage-Wise (KSW) theory for nucleon-nucleon (NN) interactions [20]. Short-range interactions are parametrized via contact terms and medium- and long-range interactions are given by pion exchanges, which are treated perturbatively. A striking feature of XEFT is that the expansion parameter for the pions is small compared to that in KSW theory for nucleons where large corrections occur at next-to-next-to-leading order in KSW power counting and the perturbative treatment of pions fails [21]. Furthermore, since the hyperfine splitting of the D^0 and D^{*0} is only about 7 MeV larger than the neutral pion mass, pions as well as the D^0 and D^{*0} mesons are treated

non-relativistically. States containing charged $D^{(*)}$ mesons, such as $D^{*+}D^-$, are integrated out, since they lie about 8 MeV above the threshold for neutral $D^{(*)}$ mesons. If they are included in the theory, they occur first at next-to-next-to-leading order (NNLO) in the power counting [21].

Ultimately, it should be possible to understand the peculiar nature of the $X(3872)$ directly from QCD. In Ref. [22], some evidence against the quantum number assignment $J^{PC} = 2^{-+}$ from a quenched lattice calculation was provided. The first lattice results for the X in full QCD were recently published by Prelovsek and Leskovec in [23]. They found a candidate for the $X(3872)$ about 11 ± 7 MeV below the $\bar{D}^0 D^{*0}$ threshold. Their simulation was performed on a relatively small lattice with a box length of approximately 2 fm and up and down quark masses of about four times the physical value. These first results underscore the importance to understand the dependence of the properties of the X on the volume and the light quark masses.

Wang and Wang used a unitarized heavy-hadron chiral perturbation theory approach with pion exchange and a contact interaction in the channel of the X [24]. They claimed that the properties of the $X(3872)$ are insensitive to the contact interaction and concluded that the binding energy of the X and its quark mass dependence are determined by pion exchange alone. This conclusion was challenged by Baru et al., who investigated the quark mass dependence within the framework of a non-relativistic Faddeev-type three-body equation with non-perturbative pions [25]. They included a $D\bar{D}\pi$ contact interaction to render the equation well defined and found that the binding energy of the X is indeed sensitive to the quark mass dependence of this term.

In this work, we calculate the light quark mass dependence of the $X(3872)$ in XEFT where pions are perturbative. To the order we are working, the quark mass dependence is synonymous to the pion mass dependence because of the Gell-Mann-Oakes-Renner relation [26]:

$$m_\pi^2 = -(m_u + m_d)\langle 0|\bar{u}u + \bar{d}d|0\rangle/f^2, \quad (3)$$

where $f \approx 130$ MeV is the pion decay constant and $\langle 0|\bar{u}u|0\rangle = \langle 0|\bar{d}d|0\rangle = (-283(2) \text{ MeV})^3$ is the light quark condensate in the \overline{MS} scheme at 2 GeV [27]. In the following, we will therefore refer only to the pion mass dependence which is more convenient for our purpose and treat the pion mass as a parameter that can be varied by adjusting the values of the quark masses.

The paper is organized as follows: In Sec. II, we review XEFT and discuss the diagrams contributing to $\bar{D}^0 D^{*0}$ scattering in the $C = +1$ channel up to NLO.¹ The issue of infrared divergences arising from on-shell pions and their treatment is discussed in Sec. III. Our results for the binding energy of the X and scattering length in the X channel are given in Sec. IV. In Sec. V, we discuss the chiral extrapolations of the binding energy and scattering length in detail. Finally, we present our conclusions and an outlook on future work in Sec. VI.

II. XEFT AND THE $\bar{D}^0 D^{*0}$ SCATTERING AMPLITUDE

The Lagrangian for XEFT was derived in Ref. [17] from heavy-hadron chiral perturbation theory. It contains non-relativistic fields for the D^0 , D^{*0} , \bar{D}^0 , and \bar{D}^{*0} mesons as well as

¹ For simplicity, we will from now on refer to this channel as the X channel.

non-relativistic pion fields. The charged D and D^* mesons have been integrated out of the theory. This can be done if one is interested in physics near the neutral threshold because the charged threshold is about 8 MeV higher in energy. This implies that typical momenta of charged mesons are of the order 120 MeV, being much larger than the typical momenta of the neutral mesons which are in the order of the binding momentum ~ 20 MeV for $E_X = 0.2$ MeV. If the charged states are not integrated out, they appear at NNLO in the power counting. Here, we work only to NLO. The interaction between the D and D^* mesons is given by pion exchange and by contact interactions in the $C = +1$ channel for $\bar{D}^0 D^{*0}$ scattering. The Lagrangian reads

$$\begin{aligned}
\mathcal{L} = & \bar{D}^\dagger \left(i\partial_0 + \frac{\vec{\nabla}^2}{2m_{D^*}} \right) \bar{D} + D^\dagger \left(i\partial_0 + \frac{\vec{\nabla}^2}{2m_D} \right) D \\
& + \bar{D}^\dagger \left(i\partial_0 + \frac{\vec{\nabla}^2}{2m_{D^*}} \right) \bar{D} + \bar{D}^\dagger \left(i\partial_0 + \frac{\vec{\nabla}^2}{2m_D} \right) \bar{D} + \pi^\dagger \left(i\partial_0 + \frac{\vec{\nabla}^2}{2m_\pi} + \delta \right) \pi \\
& + \frac{g}{\sqrt{2}f} \frac{1}{\sqrt{2}m_\pi} \left(D D^\dagger \cdot \vec{\nabla} \pi + \bar{D}^\dagger \bar{D} \cdot \vec{\nabla} \pi^\dagger \right) + \text{h.c.} \\
& - \frac{C_0}{2} (\bar{D} D + D \bar{D})^\dagger \cdot (\bar{D} D + D \bar{D}) \\
& + \frac{C_2}{16} (\bar{D} D + D \bar{D})^\dagger \cdot (\bar{D} \overleftrightarrow{\nabla}^2 D + D \overleftrightarrow{\nabla}^2 \bar{D}) + \text{h.c.} \\
& - \frac{D_2 \mu^2}{2} (\bar{D} D + D \bar{D})^\dagger \cdot (\bar{D} D + D \bar{D}) + \dots,
\end{aligned} \tag{4}$$

where $\overleftrightarrow{\nabla} \equiv \overleftarrow{\nabla} - \overrightarrow{\nabla}$ and the ellipsis denote higher order interactions. The Lagrangian (4) is invariant under charge conjugation, parity inversion, time reversal, and exhibits Galilean invariance. Moreover, $m_\pi = 135$ MeV is the neutral pion mass, $g = 0.5$ is the D meson axial coupling constant, $f = 132$ MeV is the pion decay constant, and $\Delta = m_{D^*} - m_D = 142$ MeV is the hyperfine splitting of the D^0 and D^{*0} mesons. The mass scales μ and δ are defined as $\mu^2 \equiv \Delta^2 - m_\pi^2 = (44 \text{ MeV})^2$ and $\delta \equiv \Delta - m_\pi = 7$ MeV. We treat δ as a small mass scale compared to the pion mass and expand amplitudes in δ/m_π (cf. Appendix A). The coupling constants C_0 , C_2 , and D_2 and the power counting in XEFT are discussed below. To NLO, the light quark mass dependence enters via the pion exchange and the contact interaction D_2 .

An essential feature of XEFT is the perturbative approach to include pions. By means of naive dimensional analysis, the two-pion exchange is suppressed compared to the one-pion exchange by a factor of

$$\frac{g^2 M_{DD^*} \mu}{4\pi f^2} \approx \frac{1}{20}, \tag{5}$$

which justifies the perturbative treatment of pions [17]. Besides, we expand all graphs in powers of the mass ratios $m_\pi/m_D \approx 0.07$ and $\delta/m_\pi \approx 0.04$, which are of the same order as the expansion parameter in (5). Hence, diagrams including a pion with an additional suppression factor of m_π/m_D or δ/m_π are in the same order of magnitude as the two-pion exchange graph which is of NNLO and can be neglected.²

² Note that for the calculation of the decay width of the $X(3872)$, neglecting m_π/m_D terms is not a good approximation. We will come to this issue in chapter IV D.

We have explicitly checked that corrections from relativistic pions can be neglected at NLO. Expanding these contributions around the non-relativistic limit, we find that relativistic corrections to NLO diagrams including pions are suppressed by an additional power of m_π/m_D .

Since we treat the $X(3872)$ as an S -wave hadronic molecule, the total angular momentum is given by the D^{*0} meson's spin. From angular momentum conservation thus follows that the polarizations of the incoming and outgoing D^{*0} mesons have to coincide. Using spin indices i and j , the spin dependence of the transition amplitude is of the form

$$\hat{\mathcal{A}}_{ij} = \delta_{ij} \mathcal{A}. \quad (6)$$

For the discussion of the binding energy and scattering length, it is sufficient to consider the scalar amplitude \mathcal{A} .

In XEFT power counting, the binding momentum, the D^0 and D^{*0} meson's as well as the pion's typical momentum and the scale μ are counted as order Q . All propagators are of order Q^{-2} and loops are of order Q^5 [17]. At leading-order (LO) Q^{-1} , there is only one contact term, C_0 . Note also that appending a loop (Q^5) including two $D^{(*)}$ meson propagators (Q^{-4}) and a C_0 vertex (Q^{-1}) does not change the order of any diagram. Therefore, C_0 vertices have to be resummed to all orders. Using the power divergence subtraction procedure (PDS)

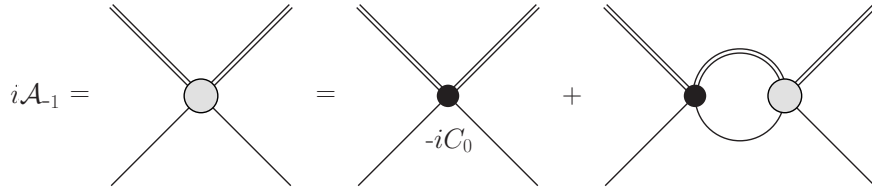


FIG. 1: Leading order contributions to the $\bar{D}^0 D^{*0}$ scattering amplitude. The \bar{D}^0 and the D^{*0} mesons are indicated by single and double lines, respectively.

[20], the LO amplitude at energy E for $\bar{D}^0 D^{*0}$ scattering in the $C = +1$ channel, depicted in Fig. 1, is given as

$$i\mathcal{A}_{-1} = \frac{2\pi i}{M_{DD^*} - \gamma + \sqrt{-2M_{DD^*}E - i\epsilon}}, \quad (7)$$

where M_{DD^*} is the reduced mass of the D^0 and D^{*0} mesons. The quantity γ is defined as

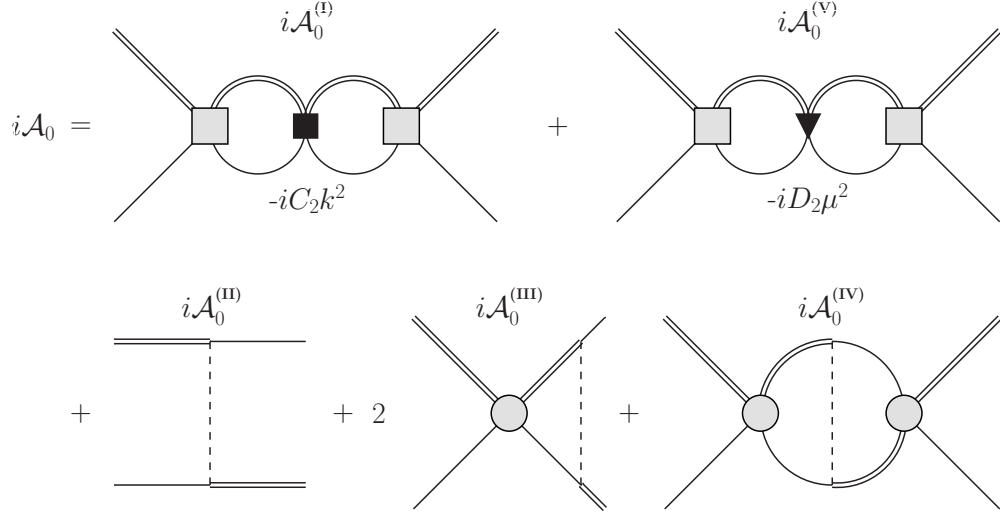
$$\gamma \equiv \frac{2\pi}{M_{DD^*}C_0(\Lambda)} + \Lambda, \quad (8)$$

with the PDS renormalization scale Λ . Taking Λ of order Q , we see that the LO amplitude indeed scales as Q^{-1} . It has a pole at the LO binding energy $E_X^{\text{LO}} = \gamma^2/(2M_{DD^*})$.³ Hence, γ can be identified with the LO binding momentum.

At order Q^0 , which is NLO in XEFT power counting, we have to include further contact interactions with coupling constants C_2 and D_2 which are both of order Q^{-2} . In the XEFT

³ After the inclusion of pions, the pole position of the scattering amplitude becomes complex and will be denoted by B . The binding energy, E_X , is then given as the real part of B .

Lagrangian (4) the coupling constant C_2 comes with two derivatives and D_2 with a factor of μ^2 . Note that this is different from the factor m_π^2 in KSW counting because in XEFT the typical momenta of the $D^{(*)}$ mesons are of order $\mu \ll m_\pi$. Vertices including C_2 or D_2 thus are of order Q^0 . For each pion exchange there are two $D^0 D^{*0} \pi^0$ axial couplings, each of order Q^1 , and one pion propagator of order Q^{-2} resulting in order Q^0 , too. We end up with the five diagrams shown in Fig. 2.



where

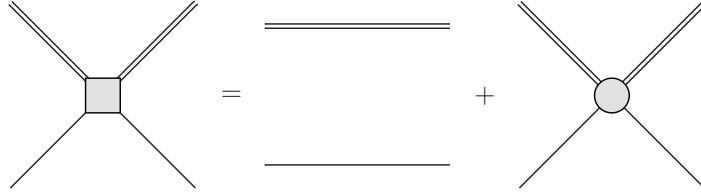


FIG. 2: Next-to-leading order contributions to the $\bar{D}^0 D^{*0}$ scattering amplitude. The pions, the \bar{D}^0 , and the D^{*0} mesons are indicated by dashed lines, solid lines, and double lines, respectively.

A novel feature of XEFT is the occurrence of a sixth diagram, $\mathcal{A}_0^{(\text{VI})}$, depicted in Fig. 3. The transition amplitude $\mathcal{A}_0^{(\text{VI})}$ comes from the self energy diagram for the D^{*0} shown in

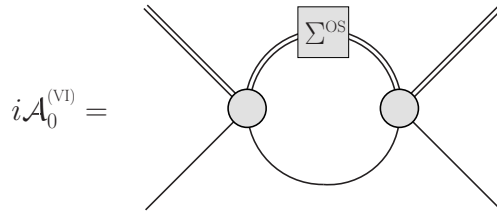


FIG. 3: NLO contribution from D^{*0} self energy. We use the same notation like in Fig. 2.

Fig. 4. It does not occur in KSW theory due to the different kinematics for nucleons.

$$i\Sigma^{\text{OS}} = \text{---}\boxed{\Sigma^{\text{OS}}}\text{---} = i\Sigma + i\delta_\Sigma = \text{---}\text{---}\text{---} + \text{---}\text{---}\text{---}$$

FIG. 4: Self energy graph and counter term for the D^{*0} . We use the same notation like in Fig. 2.

Since pions are always off-shell for the NN system, the bare self energy diagram is purely imaginary and removed by the counter term in the on-shell renormalization scheme. We will further discuss this issue in section III. We denote the external incoming momenta in the center-of-momentum frame of the D^0 and D^{*0} mesons \mathbf{p} and $-\mathbf{p}$ and the outgoing \mathbf{l} and $-\mathbf{l}$, respectively, use $p = |\mathbf{p}| = |\mathbf{l}|$ for elastic scattering and evaluate the amplitudes at on-shell energy $E = p^2/(2M_{DD^*})$. We start with the contributions of the NLO contact interactions, $\mathcal{A}_0^{(\text{I})}$ and $\mathcal{A}_0^{(\text{V})}$, respectively. Similar to the NN case [20], we acquire

$$i\mathcal{A}_0^{(\text{I})} = \frac{-iC_2p^2}{C_0^2}\mathcal{A}_{-1}^2, \quad (9a)$$

$$i\mathcal{A}_0^{(\text{V})} = \frac{-iD_2\mu^2}{C_0^2}\mathcal{A}_{-1}^2. \quad (9b)$$

The one-pion exchange transition amplitude $\hat{\mathcal{A}}_0^{(\text{II})}{}_{ij}$ is given as

$$i\hat{\mathcal{A}}_0^{(\text{II})}{}_{ij} = \frac{ig^2}{2f^2} \frac{(\boldsymbol{\varepsilon}_i \cdot \mathbf{q})(\boldsymbol{\varepsilon}_j \cdot \mathbf{q})}{\mathbf{q}^2 - \mu^2}, \quad (10)$$

where \mathbf{q} is the momentum transfer and $\boldsymbol{\varepsilon}_i$ and $\boldsymbol{\varepsilon}_j$ are the polarization vectors of the D^{*0} mesons. Projecting $\hat{\mathcal{A}}_0^{(\text{II})}{}_{ij}$ on the X channel and factoring out the spin dependence as in (6), we end up with

$$i\mathcal{A}_0^{(\text{II})} = \frac{ig^2}{6f^2} \left[1 + \frac{\mu^2}{4p^2} \log \left(1 - \frac{4p^2}{\mu^2} \right) \right]. \quad (11)$$

For the one- and two-loop diagrams with one-pion exchange, $\mathcal{A}_0^{(\text{III})}$ and $\mathcal{A}_0^{(\text{IV})}$, we acquire

$$i\mathcal{A}_0^{(\text{III})} = \frac{ig^2}{3f^2} \left[(ip + \Lambda) + i\mu^2 \frac{1}{2p} \log \left(1 + \frac{2p}{\mu} \right) \right] \frac{M_{DD^*}}{2\pi} \mathcal{A}_{-1}, \quad (12a)$$

$$i\mathcal{A}_0^{(\text{IV})} = \frac{ig^2}{6f^2} \left[(ip + \Lambda)^2 + \mu^2 \left(\log \left(\frac{\Lambda}{-2ip - i\mu} \right) + 1 + R \right) \right] \left(\frac{M_{DD^*}}{2\pi} \right)^2 \mathcal{A}_{-1}^2, \quad (12b)$$

with $R \equiv \frac{1}{2}(-\gamma_E + \log(\frac{\pi}{4}) + \frac{2}{3})$. Since $\mathcal{A}_0^{(\text{IV})}$ depends logarithmically on Λ it is required to include the μ^2 -dependent vertex proportional to D_2 to ensure that physical results are renormalization scale independent [20].

III. INFRARED DIVERGENCES AND FULL D^{*0} PROPAGATOR

For the calculation of diagram $\mathcal{A}_0^{(\text{VI})}$ in Fig. 3, we first consider the renormalized D^{*0} self energy shown in Fig. 4. Explicit calculations for the bare self energy diagram and $\mathcal{A}_0^{(\text{VI})}$ can be found in Appendix A. We use the on-shell renormalization scheme, where the counter

term, $i\delta_\Sigma$, on the right hand side of Fig. 4 is chosen such that the real part of the pole position of the D^{*0} propagator stays at the on-shell D^{*0} energy $p_0 = p^2/2m_{D^*}$. This implies that the counter term has to cancel the imaginary part of the bare self energy, $i\Sigma$, which is in the PDS renormalization scheme given as⁴

$$i\Sigma = \frac{ig^2}{24\pi f^2} (i\mu^3 + \Lambda\mu^2). \quad (13)$$

For pion masses $m_\pi > \Delta$, μ becomes imaginary, such that the bare self energy is imaginary, too. It follows for the counter term

$$i\delta_\Sigma = \begin{cases} -\frac{ig^2}{24\pi f^2} \Lambda\mu^2 & , m_\pi < \Delta, \\ -\frac{ig^2}{24\pi f^2} (i\mu^3 + \Lambda\mu^2) & , m_\pi > \Delta. \end{cases} \quad (14)$$

We see that as soon as pions can not go on-shell, the on-shell renormalized self energy yields zero and hence $\mathcal{A}_0^{(\text{VI})}$ vanishes, too. Note that pions in NN scattering are always off-shell, implying that the diagram in Fig. 3 does not contribute in KSW theory. However, for the case $m_\pi < \Delta$, we obtain

$$i\mathcal{A}_0^{(\text{VI})} = \frac{i}{p} 2\pi i\Sigma^{\text{OS}} \left(\frac{M_{DD^*}}{2\pi} \right)^2 \mathcal{A}_{-1}^2, \quad (15)$$

which is infrared divergent. The divergence occurs due to an inappropriate expansion at

$$iG = \text{---} = \text{====} + \text{====} \boxed{\Sigma^{\text{OS}}} \text{---}$$

FIG. 5: Full D^{*0} propagator. The free D^{*0} propagator is denoted by a double line, the full D^{*0} propagator by a thick, single line.

low energies. To trace the origin of the infrared divergence, let us consider the full D^{*0} propagator with resummed self energy shown in Fig. 5

$$iG = \frac{i}{p_0 - p^2/2m_{D^*} + i\epsilon} (1 + i\Sigma^{\text{OS}} iG) = \frac{i}{p_0 - p^2/2m_{D^*} + \Sigma^{\text{OS}} + i\epsilon}. \quad (16)$$

For pion masses $m_\pi < \Delta$, Σ^{OS} is purely imaginary and is related to the decay width of the D^{*0} , Γ_* , by $\Sigma^{\text{OS}} = i\Gamma_*/2$. Hence, the full propagator takes the nonzero decay width of the D^{*0} into account.

Now, we use (16) to evaluate $\mathcal{A}_0^{(\text{VI})}$ with full instead of free D^{*0} propagators. To avoid double counting, we replace one of the two free D^{*0} propagators in the loop in Fig. 3 by the

⁴ Note that taking the D^{*0} energy to be of order $p^2/m_{D^*} \sim |\Sigma^{\text{OS}}|$ and neglecting the pion loop dressed D^{*0} propagator with additional factors of m_π/m_D , the bare D^{*0} self energy is energy independent and thus the field strength renormalization constant is 1. All corrections are suppressed by $g^2 M_{DD^*} \mu / (4\pi f^2)$ times powers of m_π/m_D .

full one. This yields the resummed amplitude $\left(\mathcal{A}_0^{(\text{VI})}\right)^{\text{res}}$

$$\begin{aligned} i\left(\mathcal{A}_0^{(\text{VI})}\right)^{\text{res}} &= \frac{-2ip + 2\sqrt{-p^2 - i\kappa^2 - i\epsilon}}{i\kappa^2} 2\pi i \Sigma^{\text{OS}} \left(\frac{M_{DD^*}}{2\pi}\right)^2 \mathcal{A}_{-1}^2 \\ &= \frac{-2 + 2\sqrt{1 + i\kappa^2/p^2}}{i\kappa^2/p^2} \cdot \frac{i}{p} 2\pi i \Sigma^{\text{OS}} \left(\frac{M_{DD^*}}{2\pi}\right)^2 \mathcal{A}_{-1}^2, \end{aligned} \quad (17)$$

with $i\kappa^2 = 2M_{DD^*}\Sigma^{\text{OS}}$. As can be seen from the first line, the resummed transition amplitude is infrared finite for all values of m_π . Let us expand the first factor in the second line of (17) around $\kappa^2/p^2 = 0$, which is equivalent to expanding the full D^{*0} propagator. At zeroth order we reproduce Eq. (15). It is clear that this expansion is invalid for momenta $p \lesssim |\kappa| \approx 5$ MeV and we have to use the full D^{*0} propagator instead of the expanded one. Physically speaking, at energies close to the $\bar{D}^0 D^{*0}$ threshold, the main contribution to the loop integral comes from the low-energy regime, where the virtual D^{*0} meson can propagate much longer than the D^{*0} 's average lifetime. Therefore, it is not justified to treat its decay in perturbation theory anymore.

When dressing the D^{*0} propagators in diagrams $\mathcal{A}_0^{(\text{I})}$ to $\mathcal{A}_0^{(\text{V})}$ with pion loops, similar infrared divergences occur. Hence, for consistency, we have to use the full D^{*0} propagator for all these diagrams, as well as for the LO amplitude \mathcal{A}_{-1} . Note that the size of κ is in the order of the typical momentum scale of XEFT, Q . This implies that the full D^{*0} propagator is still of order Q^{-2} , i.e. the power counting remains unaltered.

IV. BINDING ENERGY AND SCATTERING LENGTH

The central point of this work is the calculation of low-energy observables for the X in dependence on the light quark masses. In this section we present the results for the transition amplitudes, the binding energy and the scattering length at NLO. We renormalize the transition amplitudes by use of the coupling constants C_0 , C_2 , and D_2 .

A. Transition amplitudes up to NLO

As seen in the previous section, amplitudes containing a D^{*0} propagator dressed with a pion loop exhibit infrared divergences. Therefore, considering the low-energy regime, we have to reexpress the LO and NLO amplitudes \mathcal{A}_{-1} and $\mathcal{A}_0^{(\text{I})}$ to $\mathcal{A}_0^{(\text{V})}$ with full D^{*0} propagators. Note that the LO amplitude \mathcal{A}_{-1} with the D^{*0} propagator dressed to all orders automatically includes the amplitude $\mathcal{A}_0^{(\text{VI})}$, which thus must not be taken into account separately to avoid

double counting. Skipping the superscript for convenience, the amplitudes read

$$i\mathcal{A}_{-1} = \frac{2\pi i}{M_{DD^*}} \frac{1}{-\gamma + \eta}, \quad (18a)$$

$$i\mathcal{A}_0^{(\text{I})} = \frac{-iC_2}{C_0^2} \left(p^2 + 2M_{DD^*}\Sigma^{\text{os}} \frac{-\eta + \Lambda}{-\gamma + \Lambda} \right) \mathcal{A}_{-1}^2, \quad (18b)$$

$$i\mathcal{A}_0^{(\text{II})} = \frac{ig^2}{6f^2} \left(1 + \frac{\mu^2}{4p^2} \log \left(1 - \frac{4p^2}{\mu^2} \right) \right), \quad (18c)$$

$$i\mathcal{A}_0^{(\text{III})} = \frac{ig^2}{3f^2} \left((-\eta + \Lambda) + \frac{i\mu^2}{2p} \log \left(1 + \frac{2p}{i\eta + \mu - p} \right) \right) \frac{M_{DD^*}}{2\pi} \mathcal{A}_{-1}, \quad (18d)$$

$$i\mathcal{A}_0^{(\text{IV})} = \frac{ig^2}{6f^2} \left((-\eta + \Lambda)^2 + \mu^2 \left(\log \left(\frac{\Lambda}{2\eta - i\mu} \right) + 1 + R \right) \right) \left(\frac{M_{DD^*}}{2\pi} \right)^2 \mathcal{A}_{-1}^2, \quad (18e)$$

$$i\mathcal{A}_0^{(\text{V})} = \frac{-iD_2\mu^2}{C_0^2} \mathcal{A}_{-1}^2, \quad (18f)$$

with η defined as $\eta \equiv \sqrt{-p^2 - 2M_{DD^*}\Sigma^{\text{os}} - i\epsilon}$. All diagrams are finite for $p \rightarrow 0$ for all values of m_π . For $\Sigma^{\text{os}} \rightarrow 0$, $\eta \rightarrow -ip$ and the results for the diagrams with the free D^{*0} propagator are reproduced. The LO diagram \mathcal{A}_{-1} has a pole at $p^2 = \eta_B^2 \equiv -\gamma^2 - 2M_{DD^*}\Sigma^{\text{os}}$, corresponding to an LO pole position at $-E = B^{\text{LO}} = \gamma^2/(2M_{DD^*}) + \Sigma^{\text{os}}$, which is complex for $m_\pi < \Delta$. The binding energy is given as the real part of the pole position and can be adjusted with γ for renormalization.⁵ Our result for the LO transition amplitude \mathcal{A}_{-1} is in agreement with the results from [28], where the authors obtained the $\bar{D}^0 D^{*0}$ transition amplitude to LO by analytically continuing the parameters of a threshold resonance form for two stable particles to the complex plane.

B. Renormalization of the transition amplitude

The transition amplitude $\mathcal{A}_0 = \mathcal{A}_0^{(\text{I})} + \mathcal{A}_0^{(\text{II})} + \mathcal{A}_0^{(\text{III})} + \mathcal{A}_0^{(\text{IV})} + \mathcal{A}_0^{(\text{V})}$ has to be renormalization scale independent up to NLO. It follows for the coupling constants C_2 and D_2

$$C_2 = \frac{M_{DD^*}}{2\pi} \frac{r_0}{2} (C_0)^2 \equiv c_2 (C_0)^2, \quad (19a)$$

$$D_2 = \frac{6f^2}{g^2} \left(\frac{2\pi}{M_{DD^*}} \right)^2 \left(d_2 + \log \left(\frac{\Lambda}{\mu^{\text{ph}}} \right) - R \right) (C_0)^2, \quad (19b)$$

in analogy to [20] and [17]. Here and in the following, the superscript ph denotes the physical value of a quantity, i.e. at the physical pion mass. The quantity r_0 with dimension of length can be identified with the effective range in the pionless theory. We further absorbed the constant R , which occurs in PDS, in the coupling constant D_2 . Following the arguments of [17], we use $r_0 \in [0, 1/100\text{MeV}]$, such that the maximum value of r_0 is inversely proportional to the momentum scales integrated out of the theory. For the dimensionless parameter d_2 , we use that the numerical value of the terms in the parentheses with μ^2 as prefactor in Eq. (12b) is about 0.9 evaluated at the physical pion mass with $\Lambda \sim \mu^{\text{ph}}$. We will therefore take $d_2 \in [-1, 1]$.

⁵ Since we are not considering inelastic channels like for example $X \rightarrow J/\Psi \pi^+ \pi^-$, the LO binding momentum, γ , is real valued [28].

C. The binding energy at NLO

To calculate the binding energy at NLO, we compare the XEFT result for the transition amplitude $\mathcal{A} = \mathcal{A}_{-1} + \mathcal{A}_0 + \dots$ with a generic, non-perturbative representation $\mathcal{A}^{\text{np}} = Z/(E+B) + \dots$ with shifted pole position B and field strength renormalization constant Z . The shifts for the pole position and the field strength renormalization constant can then be acquired by expanding both, the XEFT and the non-perturbative expression, around the LO pole position and matching coefficients afterwards. First, we expand the LO amplitude around the LO position of the pole and discard all terms regular at $E = -B^{\text{LO}}$, represented by ellipsis

$$\mathcal{A}_{-1} = \frac{Z_{-1}}{E + B^{\text{LO}}} + \dots \quad (20)$$

The LO field strength renormalization constant, Z_{-1} , is given as the residue at $E = -B^{\text{LO}}$

$$\Rightarrow (Z_{-1})^{-1} = \left[i \frac{\partial}{\partial E} \frac{1}{i\mathcal{A}_{-1}} \right]_{E=-B^{\text{LO}}} = \frac{-(M_{DD^*})^2}{2\pi} \frac{1}{\gamma}. \quad (21)$$

Next, we expand the amplitude \mathcal{A}_0 around the LO pole position. It divides into three parts: one proportional to \mathcal{A}_{-1} , one proportional to \mathcal{A}_{-1}^2 and one being finite at $E = -B^{\text{LO}}$ again denoted by ellipsis

$$\begin{aligned} \mathcal{A}_0 &= \left[c_2 \frac{2\pi}{M_{DD^*}} \frac{\eta_0^2}{\gamma - \Lambda} + \frac{g^2}{6f^2} \frac{M_{DD^*}}{2\pi} \frac{i\mu^2}{\eta_B} \log \left(1 + \frac{2\eta_B}{i\gamma + \mu - \eta_B} \right) \right] \mathcal{A}_{-1} + \\ &+ \left[c_2 \gamma^2 + \frac{g^2}{6f^2} \left(\frac{M_{DD^*}}{2\pi} \right)^2 \left[(\gamma - \Lambda)^2 + \mu^2 \left(-d_2 + \log \left(\frac{\mu^{\text{ph}}}{2\gamma - i\mu} \right) + 1 \right) \right] \right] \mathcal{A}_{-1}^2 + \dots \\ &\equiv s_1 \cdot \frac{Z_{-1}}{E + B^{\text{LO}}} + s_2 \cdot \frac{Z_{-1}^2}{(E + B^{\text{LO}})^2} + \dots, \end{aligned} \quad (22)$$

where $\eta_0 \equiv \sqrt{-2M_{DD^*}\Sigma^{\text{os}}}$. The terms linear in \mathcal{A}_{-1} arise due to cancellations in the numerator at $E = -B^{\text{LO}}$. We now compare the non-perturbative expression \mathcal{A}^{np} at energy $B = B^{\text{LO}} + \Delta B$ with field strength renormalization constant $Z = Z_{-1} + \Delta Z$ to the XEFT result \mathcal{A}

$$\mathcal{A} = \mathcal{A}_{-1} + \mathcal{A}_0 + \dots = \frac{Z_{-1} + s_1 Z_{-1}}{E + B^{\text{LO}}} + \frac{s_2 Z_{-1}^2}{(E + B^{\text{LO}})^2} + \dots, \quad (23a)$$

$$\mathcal{A}^{\text{np}} = \frac{Z}{E + B} + \dots = \frac{Z_{-1} + \Delta Z}{E + B^{\text{LO}}} - \frac{Z\Delta B}{(E + B^{\text{LO}})^2} + \dots \quad (23b)$$

The shift of the field strength renormalization constant and the pole position to NLO can then be read off by equating the corresponding coefficients

$$\Delta Z^{\text{NLO}} = s_1 Z_{-1}, \quad (24a)$$

$$\Delta B^{\text{NLO}} = -\frac{Z_{-1}^2}{Z_{-1} + \Delta Z} s_2 = -\frac{Z_{-1}}{1 + s_1} s_2. \quad (24b)$$

The superscript denotes that these relations hold up to NLO. In summary, the binding energy E_X is given as

$$E_X = \text{Re} [B^{\text{LO}} + \Delta B^{\text{NLO}}], \quad (25a)$$

$$B^{\text{LO}} + \Delta B^{\text{NLO}} = \frac{\gamma^2}{2M_{DD^*}} + \Sigma^{\text{os}} - \frac{Z_{-1}}{1+s_1}s_2, \quad (25b)$$

$$Z_{-1} = -\frac{2\pi\gamma}{(M_{DD^*})^2}, \quad (25c)$$

$$s_1 = c_2 \frac{2\pi}{M_{DD^*}} \frac{\eta_0^2}{\gamma - \Lambda} + \frac{g^2}{6f^2} \frac{M_{DD^*}}{2\pi} \frac{i\mu^2}{\eta_B} \log \left(1 + \frac{2\eta_B}{i\gamma + \mu - \eta_B} \right), \quad (25d)$$

$$s_2 = c_2 \gamma^2 + \frac{g^2}{6f^2} \left(\frac{M_{DD^*}}{2\pi} \right)^2 \left[(\gamma - \Lambda)^2 + \mu^2 \left(-d_2 + \log \left(\frac{\mu^{\text{ph}}}{2\gamma - i\mu} \right) + 1 \right) \right]. \quad (25e)$$

For renormalization, we fix it at the physical value of the pion mass and use $E_X^{\text{ph}} = 0.2$ MeV. This defines a relation between the LO binding momentum γ , i.e. C_0 , and the coefficients c_2 and d_2 .

D. The imaginary part of the pole position

The imaginary part of the pole position $B = B^{\text{LO}} + \Delta B^{\text{NLO}}$ can be obtained by cutting the diagrams in Figs. 1 and 2 with the free D^{*0} propagator replaced with the full one. Consider for example the cut diagrams shown in Fig. 6. Note that the first diagram is included in the LO amplitude \mathcal{A}_{-1} . Applying the cuts by replacing all cut propagators with appropriate delta distributions and keeping all m_π/m_D suppressed terms, the expressions for the imaginary parts coincide with the decay diagrams in [28] at energy E_X . In [17], the

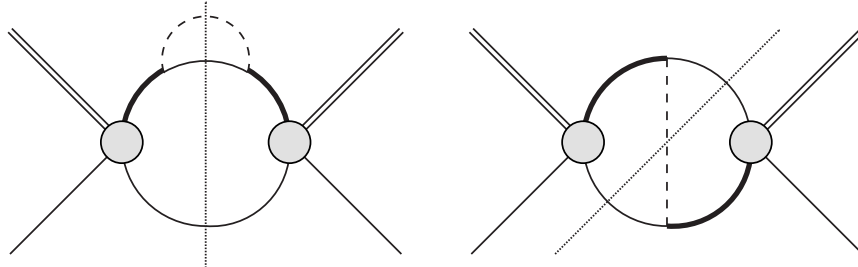


FIG. 6: Cut diagrams, determining the imaginary part of the pole position B . We use the same notation as in the previous figures. The cuts through the pion, D^0 and \bar{D}^0 meson propagators are indicated by dotted lines.

authors pointed out that dropping m_π/m_D terms is equivalent to treating pions in potential approximation.⁶ But for the decay diagrams, the pions in the final state are on-shell and

⁶ For potential pions, the kinetic energy is much smaller than the pion momentum [29]. Dropping m_π/m_D terms implies that the kinetic energy of the pions is neglected and thus pions are treated in potential approximation.

the potential approximation is invalid. Hence, for the calculation of the imaginary part of the pole position, which is related to the decay width by $\text{Im}[B] = \Gamma[X \rightarrow D^0 \bar{D}^0 \pi^0]/2$, all m_π/m_D suppressed terms have to be kept and the remaining three-body phase space integral has to be evaluated numerically. It is not to be expected that the decay width is well approximated when treating the final state pions in potential approximation. Further discussions can be found in [8, 17, 28].

E. The scattering length at NLO

In the previous chapters we presented results for the transition amplitudes and derived an expression for the binding energy at LO and NLO. We now turn to the calculation of the scattering length. For this purpose we consider the S -matrix which is related to the S -wave transition amplitude \mathcal{A} by

$$S - 1 = e^{2i\delta_s} - 1 = i \frac{p M_{DD^*}}{\pi} \mathcal{A}, \quad (26)$$

with the S -wave scattering phase shift δ_s . To take the inelastic channel $DD^* \rightarrow \bar{D}D\pi$ into account, we allow the scattering phase shift to be complex. Equation (26) can be rewritten and expanded at low energies in p^2 as

$$p \cot \delta_s = ip + \frac{2\pi}{M_{DD^*} \mathcal{A}} = -\frac{1}{a_s} + \frac{1}{2} r_s p^2 + \dots, \quad (27)$$

which is known as effective range expansion. The quantity r_s is called S -wave effective range and a_s is the S -wave scattering length. In the pionless theory, the effective range r_s coincides with r_0 in Eq. (19a). However, after the inclusion of pions, the effective range expansion remains valid only up to order p^0 for $m_\pi < \Delta$ ($\mu^2 > 0$). This can be understood by taking a closer look at the Fourier transform of the one-pion exchange in potential approximation

$$\frac{g^2}{2f^2} \frac{(\boldsymbol{\varepsilon}_i \cdot \mathbf{q})(\boldsymbol{\varepsilon}_j \cdot \mathbf{q})}{\mathbf{q}^2 - \mu^2} \xrightarrow{\text{F.T.}} \frac{g^2}{8\pi f^2} (\boldsymbol{\varepsilon}_i \cdot \boldsymbol{\varepsilon}_j - 3(\boldsymbol{\varepsilon}_i \cdot \hat{\mathbf{r}})(\boldsymbol{\varepsilon}_j \cdot \hat{\mathbf{r}})) \frac{\cos(\mu r) + \mu r \sin(\mu r)}{r^3} + \dots, \quad (28)$$

occurring in all diagrams involving pions. In contrast to the exponentially decreasing potential for the one-pion exchange as an effective NN interaction, the potential (28) is oscillatory and hence the effective range r_s is not defined [30]. This results in the emergence of terms linear in p when expanding the transition amplitude around $p = 0$. Nevertheless, the S -wave scattering length is well-defined and can be extracted.

To do this, we take the limit $p \rightarrow 0$ of the transition amplitude. At NLO we acquire

$$\begin{aligned} a_s &= \frac{-M_{DD^*}}{2\pi} (\mathcal{A}_{-1} + \mathcal{A}_0) \\ &= \frac{1}{\gamma - \eta_0} - \frac{1}{(\gamma - \eta_0)^2} \left[\frac{r_0}{2} \eta_0^2 \frac{\eta_0 - \Lambda}{\gamma - \Lambda} + \frac{M_{DD^*}}{2\pi} \frac{g^2}{6f^2} \left((\gamma - \Lambda)^2 - (\gamma - \eta_0)^2 + \right. \right. \\ &\quad \left. \left. + 2\mu^2 \frac{\gamma - \eta_0}{i\mu - \eta_0} + \mu^2 \left(-d_2 + \log \left(\frac{\mu^{\text{ph}}}{2\eta_0 - i\mu} \right) + 1 \right) \right) \right]. \end{aligned} \quad (29)$$

The scattering length is complex for $m_\pi < \Delta$ and real as soon as the hyperfine splitting of the D^0 and D^{*0} mesons is smaller than the neutral pion mass.

V. CHIRAL EXTRAPOLATIONS AND RESULTS

For the determination of the quark mass dependence of the binding energy of the X , we need the chiral extrapolations of the pion decay constant, the D meson axial coupling constant and the D^0 and D^{*0} meson, respectively. We use a superscript (0) to denote the chiral limit value of a quantity. We take the m_π dependence of the pion decay constant from [31]

$$f = f^{(0)} \left[1 - \frac{1}{4\pi^2 f^{(0)2}} m_\pi^2 \log \left(\frac{m_\pi}{m_\pi^{\text{ph}}} \right) + \frac{\bar{l}_4}{8\pi^2 f^{(0)2}} m_\pi^2 \right], \quad (30)$$

with the low-energy constant $\bar{l}_4 = 4.4$ and $f^{(0)} = 124$ MeV, implying $f^{\text{ph}} = 132$ MeV [31, 32]. For the D meson axial coupling constant, we use the recent lattice results from [33]. The chiral extrapolation reads

$$g = g^{(0)} \left[1 - \frac{1 + 2g^{(0)2}}{4\pi^2 f^{(0)2}} m_\pi^2 \log \left(\frac{m_\pi}{\mu_{\text{lat}}} \right) + \alpha m_\pi^2 \right], \quad (31)$$

with the parameters [33]

$$g^{(0)} = 0.46, \quad \alpha = -0.16 \text{ GeV}^{-2}, \quad \mu_{\text{lat}} = 1 \text{ GeV}. \quad (32)$$

Evaluated at the physical pion mass, the physical value of the D meson axial coupling constant is $g^{\text{ph}} = 0.5$.

For the quark mass dependence of the D meson masses and hence the hyperfine splitting Δ , we use the results of [34]

$$m_{D^{(*)}} = m_{D^{(*)}}^{\text{ph}} + \frac{h_1}{m_{D^{(*)}}^{\text{ph}}} \left(m_\pi^2 - (m_\pi^{\text{ph}})^2 \right), \quad (33)$$

with $h_1 = 0.42$ [34].

In the KSW theory for NN scattering, the relative size of the two-pion and one-pion exchange graphs is about $1/2$. Due to NNLO coefficients of order $5 \sim 6$ being much greater than the expansion parameter in KSW theory, contributions at NLO and NNLO are of comparable magnitude and the perturbative treatment of pions fails [21]. In XEFT, the two-pion exchange is more strongly suppressed. However, the estimate of the suppression based on (5) depends on the quark mass, dominantly through the mass scale μ . To determine a region of validity for XEFT we use a rather conservative estimate for the upper bound of the expansion parameter and require that the absolute value of (5) is smaller than 0.15. Even though unnaturally large NNLO coefficients of similar size as in KSW occur, (5) is expected to be small enough to compensate for that and the perturbative inclusion of pions remains valid. For the lower bound we consider that pions are treated non-relativistically in XEFT. We require for the maximum pion velocity $v_\pi \approx \mu/m_\pi \lesssim 0.35$. These conditions are fulfilled for $0.98 (m_\pi^{\text{ph}})^2 \lesssim m_\pi^2 \lesssim 2 (m_\pi^{\text{ph}})^2$. Since the coupling constants c_2 and d_2 are undetermined, it might be that unnaturally large corrections to the LO amplitude occur at NLO. We will come to this issue when discussing the scattering length.

In Fig. 7, the quark mass dependence of the binding energy of the X is shown. We plot against the squared pion mass, which is proportional to the light quark masses at leading-order in chiral perturbation theory. Since in XEFT power counting $\Lambda \gtrsim Q$, we

use $\Lambda = 50$ MeV. As described in section IV C, we fix the binding energy at the physical value of the pion mass m_π^{ph} and use $E_X^{\text{ph}} = 0.2$ MeV. The m_π -dependent and independent contact interactions at NLO can be tuned by modifying the parameters d_2 and r_0 defined in Eqs. (19b, 19a), respectively. For $d_2 = 0$ and $r_0 = 0$, the D mesons interact via the LO contact interaction and pion exchanges only, corresponding to the solid, thick curve in Fig. 7. We see that for increasing pion mass the binding energy first moves towards the threshold with an inflection point at $m_\pi = \Delta$. Shortly after the inflection point, the sign of the slope reverses and the binding energy increases for increasing quark masses. Tuning

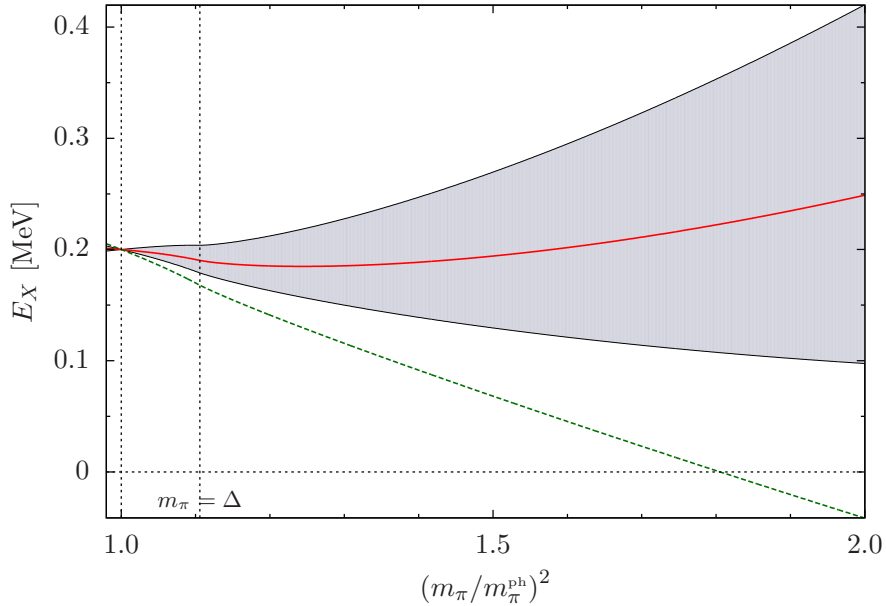


FIG. 7: Binding energy of the $X(3872)$. The solid, thick curve belongs to $d_2 = 0$ and $r_0 = 0$, i.e. considering the LO contact interaction and pion exchanges only. For $d_2 = -1$ and $r_0 = 0.01/\text{MeV}$ we acquire the lower bound and for $d_2 = 1$ and $r_0 = 0$ the upper bound for the binding energy. The dashed, thick curve corresponds to $d_2 = -2$.

the strengths of the NLO contact interactions via the parameters d_2 and r_0 can either imply that the slope of the binding energy of the X enlarges or decreases. The lower bound for the binding energy is acquired for $d_2 = -1$ and $r_0 = 0.01/\text{MeV}$. For this scenario, the binding energy remains below the physical one for pion masses $(m_\pi^{\text{ph}})^2 < m_\pi^2 < 2(m_\pi^{\text{ph}})^2$. On the other hand, assuming positive values for d_2 and small values for r_0 , the binding energy of the X steeply rises for pion masses beyond the inflection point. The upper bound belongs to $d_2 = 1$ and $r_0 = 0$. The dominating contribution to the shift of the binding energy at NLO is the quark mass dependent contact interaction. Considering, e.g., an unnaturally large and negative coupling constant d_2 , it is possible that the bound state of the X vanishes at higher quark masses. This is represented by the dashed, thick curve in Fig. 7 belonging to $d_2 = -2$ and $r_0 = 0$.

Before we consider the chiral extrapolation of the real part of the scattering length over the whole range of validity, let us take a closer look at its behavior around $m_\pi = \Delta$, i.e. where the pion mass is close to the hyperfine splitting of the D^0 and D^{*0} . At LO the

scattering length reads

$$a^{\text{LO}} = \frac{1}{\gamma - \eta_0} = \frac{1}{\gamma - \sqrt{-2i \frac{M_{DD^*} g^2}{24\pi f^2} \mu^{\frac{3}{2}} \theta(\Delta - m_\pi)}}. \quad (34)$$

For $m_\pi \rightarrow \Delta$, $\eta_0 \rightarrow 0$ and therefore $a^{\text{LO}} \rightarrow 1/\gamma$. The scattering length is continuous but not differentiable at $m_\pi = \Delta$. We consider the derivative of the real part of the scattering length with respect to m_π around $m_\pi = \Delta$ ($\mu = 0$):

$$\frac{\partial \text{Re}[a^{\text{LO}}]}{\partial m_\pi} = \begin{cases} -\frac{3}{2} \frac{m_\pi}{\gamma^2} \sqrt{\frac{M_{DD^*} g^2}{24\pi f^2}} \frac{1}{\sqrt{\mu}} + \mathcal{O}(\mu) & , m_\pi < \Delta, \\ 0 & , m_\pi > \Delta, \end{cases} \quad (35)$$

i.e. the derivative is discontinuous at $m_\pi = \Delta$. It diverges to $-\infty$ for $m_\pi \nearrow \Delta$ and is zero for $m_\pi > \Delta$. This leads to a cusp effect for the scattering length at LO.

At NLO the cusp effect is smeared out due to the logarithmic term in $\mathcal{A}_0^{(\text{III})}$. Its contribution to the scattering length reads

$$a_{(\text{III})}^{\text{NLO}} = -\frac{M_{DD^*} g^2}{6\pi f^2} \mu^2 \frac{1}{(i\mu - \eta_0)(\gamma - \eta_0)}. \quad (36)$$

Using $\mu = i|\mu|$ for $m_\pi > \Delta$, it follows for the derivative of the real part with respect to m_π

$$\frac{\partial \text{Re}[a_{(\text{III})}^{\text{NLO}}]}{\partial m_\pi} = \begin{cases} -6 \frac{m_\pi}{\gamma} \sqrt{\frac{M_{DD^*} g^2}{24\pi f^2}}^3 \frac{1}{\sqrt{\mu}} + \mathcal{O}(\mu^0) & , m_\pi < \Delta, \\ -3 \frac{m_\pi}{\gamma} \frac{M_{DD^*} g^2}{24\pi f^2} \frac{1}{|\mu|} & , m_\pi > \Delta. \end{cases} \quad (37)$$

This implies that at NLO the derivative of the real part of the scattering length diverges to $-\infty$ for both limits, $m_\pi \nearrow \Delta$ and $m_\pi \searrow \Delta$.

The real part of the scattering length in dependence on the light quark masses is shown in Fig. 8. We see the expected negative correlation between the scattering length and the binding energy, i.e. that the scattering length decreases for increasing binding energy and vice versa. Again the solid, thick curve belongs to the case where $d_2 = 0$ and $r_0 = 0$ and only the LO contact interaction and the pion exchanges are considered. The magnified area shows the smeared out cusp at $m_\pi = \Delta$ in more detail. The lower and upper bounds are obtained by varying d_2 and r_0 in the natural ranges $r_0 \in [0, 1/100\text{MeV}]$, $d_2 \in [-1, 1]$ and maximizing the width of the error band. The scattering length is unnaturally large for all values of m_π . It is therefore expected, that XEFT power counting remains valid for pion masses beyond the physical one.

VI. CONCLUSION AND OUTLOOK

In this work, we have investigated the light quark mass dependence of the $X(3872)$ to NLO in XEFT where pions are included perturbatively. We demonstrated that transition amplitudes containing dressed D^{*0} propagators as subdiagrams exhibit infrared divergences and eliminated these divergences by using full D^{*0} propagators. Moreover, we have calculated $\bar{D}^0 D^{*0}$ scattering in the X channel and gave analytical expressions for the binding energy of the $X(3872)$ and the $\bar{D}^0 D^{*0}$ scattering length at NLO in Eqs. (25) and (29).

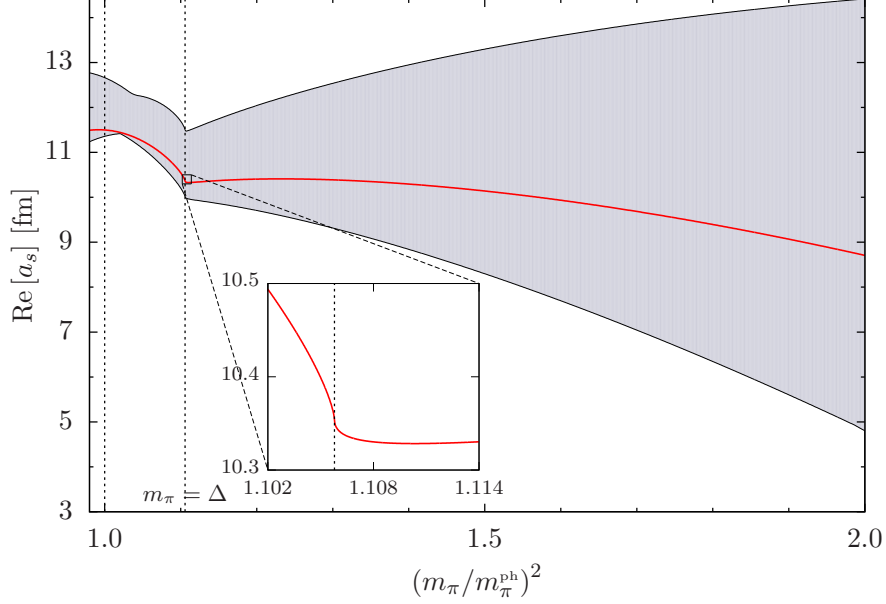


FIG. 8: The quark mass dependence of the real part of the $X(3872)$'s scattering length. The solid, thick curve belongs to $d_2 = 0$ and $r_0 = 0$. The bounds are acquired by varying d_2 and r_0 in their natural ranges $r_0 \in [0, 1/100\text{MeV}]$ and $d_2 \in [-1, 1]$ and maximizing the width of the error band.

At this order, the quark mass dependence of the X is determined by the quark mass dependence of the $D^{(*)}$ masses, of the pion exchange interaction as well as a quark mass dependent contact interaction that is required for consistent renormalization. In analogy to the NN case [20], our calculations demonstrate that it is essential to include such a term at NLO to obtain renormalization scale independent transition amplitudes. This invalidates the claim of Wang and Wang [24] that the properties of the $X(3872)$ are determined by pion exchange alone. A similar conclusion was reached by Baru et al. [25] in a Faddeev-approach with a $D\bar{D}\pi$ contact interaction.

Taking the quark mass dependence into account, there are two unknown constants r_0 and d_2 from contact interactions in the expressions for the binding energy and scattering length at NLO. While r_0 could be determined by scattering data in the X channel, the parameter d_2 , which governs the quark mass dependence of the NLO contact interaction, can only be determined on the lattice. We constrained these coupling constants by dimensional analysis arguments and examined different scenarios for their values. We found that it is most likely that the $X(3872)$ is bound for quark masses larger than the physical one. However, for an unnaturally large and negative coupling constant d_2 , a disappearance of the bound state for increasing quark masses is also possible. The qualitative behavior of the binding energy is in agreement with the results of Baru et al. [25].

Our predictions could be used to extrapolate lattice calculations of the $X(3872)$ at unphysical quark masses to the physical ones. Based on a conservative estimate of higher order effects, our results should be applicable in the region $0.98 (m_\pi^{\text{ph}})^2 \lesssim m_\pi^2 \lesssim 2 (m_\pi^{\text{ph}})^2$, where m_π^{ph} is the physical pion mass. Our results suggest that it should be possible to find the X in lattice simulations at quark masses in this region. Depending on the values of d_2 and r_0 , it can be more or less bound at larger quark masses. The first lattice results for the X in full QCD were recently provided by Prelovsek and Leskovec [23]. In a relatively small box

with $L \approx 2$ fm, they found a candidate for the $X(3872)$ about 11 ± 7 MeV below the $\bar{D}^0 D^{*0}$ threshold for a pion mass about twice the physical value and thus slightly beyond the range of applicability of our calculation. If it is nevertheless extrapolated to larger pion masses and finite volume effects are neglected, our result is consistent with the value of Prelovsek and Leskovec at the two sigma level. If simulations for multiple smaller pion masses are carried out in the future, our calculations could be used to extrapolate the lattice results to the physical values.

In the future, it would be interesting to extend our work to NNLO. At this order charged $D^{(*)}$ mesons will appear for the first time and lead to coupled channel effects if they are not integrated out of the theory. Furthermore, relativistic correction for the pions will appear and m_π/m_D corrections in NLO diagrams have to be considered. Given the small volumes currently available, it would also be useful to explicitly calculate finite volume effects in the binding energy and other observables within XEFT.

Acknowledgments

We thank C. Hanhart and U.-G. Meißner for helpful discussions. This research was supported in part by the DFG and the NSFC through funds provided to the Sino-German CRC 110, by the BMBF under grant 05P12PDFTE, by the NNSFC under grant 10935012, and by the Helmholtz Association under contract HA216/EMMI.

Appendix A: Calculation of the D^{*0} self energy and $\mathcal{A}_0^{(\text{VI})}$

In this section we show the explicit calculations for the diagrams depicted in Figs. 3 and 4. We start with the bare D^{*0} self energy diagram with spin indices i and j

$$i\hat{\Sigma}_{ij} = \left(\frac{\Lambda}{2}\right)^{4-D} \int \frac{d^D q}{(2\pi)^D} \frac{-g^2}{2f^2} \frac{1}{2m_\pi - q_0 - q^2/2m_D + i\epsilon} \frac{i}{p_0 + q_0 - (\mathbf{p} + \mathbf{q})^2/2m_\pi + \delta + i\epsilon} \frac{i(\boldsymbol{\varepsilon}_i \cdot (\mathbf{p} + \mathbf{q}))(\boldsymbol{\varepsilon}_j \cdot (\mathbf{p} + \mathbf{q}))}{(A.1)}$$

Performing the contour integration for q_0 we acquire

$$i\hat{\Sigma}_{ij} = \frac{-ig^2}{2f^2} \frac{1}{2m_\pi} \left(\frac{\Lambda}{2}\right)^{4-D} \int \frac{d^{D-1} q}{(2\pi)^{D-1}} \frac{(\boldsymbol{\varepsilon}_i \cdot (\mathbf{p} + \mathbf{q}))(\boldsymbol{\varepsilon}_j \cdot (\mathbf{p} + \mathbf{q}))}{p_0 - q^2/2m_D - (\mathbf{p} + \mathbf{q})^2/2m_\pi + \delta + i\epsilon}. \quad (A.2)$$

Using the rotational invariance of (A.2) we can replace

$$\boldsymbol{\varepsilon}_i \cdot (\mathbf{p} + \mathbf{q}) \boldsymbol{\varepsilon}_j \cdot (\mathbf{p} + \mathbf{q}) = (\mathbf{p} + \mathbf{q})_i \cdot (\mathbf{p} + \mathbf{q})_j \rightarrow \frac{\delta_{ij}}{D-1} (\mathbf{p} + \mathbf{q})^2 \quad (A.3)$$

in the integral and obtain for the self energy diagram

$$i\hat{\Sigma}_{ij} = \frac{ig^2}{2f^2} \frac{\delta_{ij}}{D-1} \left(\frac{\Lambda}{2}\right)^{4-D} \int \frac{d^{D-1} q}{(2\pi)^{D-1}} \frac{(\mathbf{p} + \mathbf{q})^2}{2m_\pi p_0 - q^2 m_\pi/m_D - (\mathbf{p} + \mathbf{q})^2 + 2m_\pi \delta + i\epsilon}. \quad (A.4)$$

The energy of the D^{*0} meson is of order $p^2/2m_{D^*}$. As explained in section II, diagrams including a pion with additional m_π/m_D suppression are in the same order as the two-pion exchange graph which occurs at NNLO first and can be neglected. We further use that

$2m_\pi\delta = \mu^2 + \mathcal{O}(\delta/m_\pi)$. Similar to (6) we utilize $i\hat{\Sigma}_{ij} = \delta_{ij}i\Sigma$. The self energy $i\Sigma$ is therefore approximately given as

$$\begin{aligned} i\Sigma &\approx -\frac{ig^2}{2f^2} \frac{1}{D-1} \left(\frac{\Lambda}{2}\right)^{4-D} \int \frac{d^{D-1}q}{(2\pi)^{D-1}} \frac{(\mathbf{p}+\mathbf{q})^2}{(\mathbf{p}+\mathbf{q})^2 - \mu^2 - i\epsilon} \\ &= -\frac{ig^2}{2f^2} \frac{1}{D-1} \left(\frac{\Lambda}{2}\right)^{4-D} \frac{1}{(4\pi)^{(D-1)/2}} \frac{D-1}{2} \Gamma\left[\frac{1-D}{2}\right] (-\mu^2 - i\epsilon)^{\frac{D-1}{2}}. \end{aligned} \quad (\text{A.5})$$

In PDS renormalization scheme, we have to remove all poles in 3 and 4 dimensions. Taking the limit $D \rightarrow 4$ we end up with

$$i\Sigma = \frac{ig^2}{24\pi f^2} (i\mu^3 + \Lambda\mu^2). \quad (\text{A.6})$$

Using on-shell renormalization, the counter term has to remove the imaginary part of $i\Sigma$. This implies for the on-shell renormalized self energy

$$i\Sigma^{\text{OS}} = \begin{cases} -\frac{ig^2}{24\pi f^2} i\mu^3, & m_\pi < \Delta, \\ 0, & m_\pi \geq \Delta. \end{cases} \quad (\text{A.7})$$

It follows for the transition amplitude $\mathcal{A}_0^{(\text{VI})}$ in Fig. 3, utilizing the previous results

$$\begin{aligned} i\mathcal{A}_0^{(\text{VI})} &= i\mathcal{A}_{-1} \left(\frac{\Lambda}{2}\right)^{4-D} \int \frac{d^D q}{(2\pi)^D} \left(\frac{i}{E + q_0 - q^2/2m_{D^*} + i\epsilon} \right)^2 i\Sigma^{\text{OS}} \frac{i}{-q_0 - q^2/2m_D} i\mathcal{A}_{-1} \\ &= i\mathcal{A}_{-1}^2 \Sigma^{\text{OS}} \left(\frac{\Lambda}{2}\right)^{4-D} \int \frac{d^{D-1}q}{(2\pi)^{D-1}} \left(\frac{2M_{DD^*}}{q^2 - p^2 - i\epsilon} \right)^2 \\ &= i\mathcal{A}_{-1}^2 (2M_{DD^*})^2 \Sigma^{\text{OS}} \left(\frac{\Lambda}{2}\right)^{4-D} \frac{1}{(4\pi)^{(D-1)/2}} \Gamma\left[\frac{5-D}{2}\right] (-p^2 - i\epsilon)^{\frac{D-5}{2}}. \end{aligned} \quad (\text{A.8})$$

This expression is ultraviolet finite in 3 and 4 dimensions. In the limit $D \rightarrow 4$ we acquire the result given in Eq. (15).

-
- [1] N. Brambilla, S. Eidelman, B. Heltsley, R. Vogt, G. Bodwin, et al., Eur. Phys. J. C **71**, 1534 (2011), 1010.5827.
 - [2] S. Choi et al. (Belle Collaboration), Phys. Rev. Lett. **91**, 262001 (2003), hep-ex/0309032.
 - [3] D. Acosta et al. (CDF Collaboration), Phys. Rev. Lett. **93**, 072001 (2004), hep-ex/0312021.
 - [4] B. Aubert et al. (BaBar Collaboration), Phys. Rev. D **74**, 071101 (2006), hep-ex/0607050.
 - [5] R. Aaij et al. (LHCb collaboration), Phys. Rev. Lett. **110**, 222001 (2013), 1302.6269.
 - [6] F. E. Close and P. R. Page, Phys. Lett. B **578**, 119 (2004), hep-ph/0309253.
 - [7] S. Pakvasa and M. Suzuki, Phys. Lett. B **579**, 67 (2004), hep-ph/0309294.
 - [8] M. Voloshin, Phys. Lett. B **579**, 316 (2004), hep-ph/0309307.
 - [9] C.-Y. Wong, Phys. Rev. C **69**, 055202 (2004), hep-ph/0311088.
 - [10] E. Braaten and M. Kusunoki, Phys. Rev. D **69**, 074005 (2004), hep-ph/0311147.

- [11] E. S. Swanson, Phys. Lett. B **588**, 189 (2004), hep-ph/0311229.
- [12] J. Beringer et al. (Particle Data Group), Phys. Rev. D **86**, 010001 (2012).
- [13] E. Braaten and H.-W. Hammer, Phys. Rept. **428**, 259 (2006), cond-mat/0410417.
- [14] E. Braaten, PoS **EFT09**, 065 (2009).
- [15] V. Baru, A. Filin, C. Hanhart, Y. Kalashnikova, A. Kudryavtsev, et al., Phys. Rev. D **84**, 074029 (2011), 1108.5644.
- [16] D. L. Canham, H.-W. Hammer, and R. P. Springer, Phys. Rev. D **80**, 014009 (2009), 0906.1263.
- [17] S. Fleming, M. Kusunoki, T. Mehen, and U. van Kolck, Phys. Rev. D **76**, 034006 (2007), hep-ph/0703168.
- [18] S. Fleming and T. Mehen, Phys. Rev. D **85**, 014016 (2012), 1110.0265.
- [19] E. Braaten, H.-W. Hammer, and T. Mehen, Phys. Rev. D **82**, 034018 (2010), 1005.1688.
- [20] D. B. Kaplan, M. J. Savage, and M. B. Wise, Phys. Lett. B **424**, 390 (1998), nucl-th/9801034.
- [21] S. Fleming, T. Mehen, and I. W. Stewart, Nucl. Phys. A **677**, 313 (2000), nucl-th/9911001.
- [22] Y.-B. Yang, Y. Chen, L.-C. Gui, C. Liu, Y.-B. Liu, et al., Phys. Rev. D **87**, 014501 (2013), 1206.2086.
- [23] S. Prelovsek and L. Leskovec (2013), 1307.5172.
- [24] P. Wang and X. Wang, Phys. Rev. Lett. **111**, 042002 (2013), 1304.0846.
- [25] V. Baru, E. Epelbaum, A. Filin, C. Hanhart, U. G. Meißner, et al., Phys. Lett. B **726**, 537 (2013), 1306.4108.
- [26] M. Gell-Mann, R. Oakes, and B. Renner, Phys. Rev. **175**, 2195 (1968).
- [27] C. McNeile, A. Bazavov, C. Davies, R. Dowdall, K. Hornbostel, et al., Phys. Rev. D **87**, 034503 (2013), 1211.6577.
- [28] E. Braaten and J. Stapleton, Phys. Rev. D **81**, 014019 (2010), 0907.3167.
- [29] T. Mehen and I. W. Stewart, Nucl. Phys. A **665**, 164 (2000), nucl-th/9901064.
- [30] M. Suzuki, Phys. Rev. D **72**, 114013 (2005), hep-ph/0508258.
- [31] J. Gasser and H. Leutwyler, Annals Phys. **158**, 142 (1984).
- [32] G. Colangelo, J. Gasser, and H. Leutwyler, Nucl. Phys. B **603**, 125 (2001), hep-ph/0103088.
- [33] D. Becirevic and F. Sanfilippo, Phys. Lett. B **721**, 94 (2013), 1210.5410.
- [34] F.-K. Guo, C. Hanhart, and U.-G. Meißner, Eur. Phys. J. A **40**, 171 (2009), 0901.1597.